MOL #58834

ANALGESIC ω-CONOTOXINS CVIE AND CVIF SELECTIVELY AND VOLTAGE DEPENDENTLY BLOCK RECOMBINANT AND NATIVE N-TYPE CALCIUM CHANNELS

G. Berecki, L. Motin, A. Haythornthwaite, S. Vink, P. Bansal, R. Drinkwater, C.I. Wang, M. Moretta, R.J. Lewis, P.F. Alewood, M.J. Christie, D.J. Adams

The Queensland Brain Institute (G.B., L.M., D.J.A.), the School of Biomedical Sciences (G.B., A.H., D.J.A.), and Institute for Molecular Bioscience (S.V., P.B., C.I.W., R.J.L., P.F.A.), The University of Queensland, Queensland 4072, Australia, Xenome Ltd, Indooroopilly, Queensland 4069, Australia (R.D.), and Brain and Mind Research Institute, University of Sydney, NSW 2006, Australia (M.M., M.J.C.)

Present address G. B.: Department of Physiology and Pharmacology, Hotchkiss Brain Institute, University of Calgary, HRIC 1A25A, 3330 Hospital Drive NW, T2N4N1 Calgary, Alberta, Canada.

Present address D.J.A.: Health Innovations Research Institute, RMIT University, PO Box 71, Bundoora, Victoria 3083 Australia.

1

MOL #58834

Running title:

ANALGESIC CVIE AND CVIF BLOCK N-TYPE CALCIUM CHANNELS

Address correspondence to: G. Berecki, Department of Physiology and Pharmacology, Hotchkiss

Brain Institute, University of Calgary, HRIC 1A25A, 3330 Hospital Dr. N.W., Calgary, Alberta,

CANADA T2N4N1. Tel. +1-403-2206597; E-mail: gberecki@ucalgary.ca

Number of text pages: 36

Number of tables: 1

Number of figures: 9

Number of references: 40

Number of words in the *Abstract*: 250

Number of words in the *Introduction*: 508

Number of words in the *Discussion*: 1489

Abbreviations: CVIE, ω-conotoxin CVIE; CVIF, ω-conotoxin CVIF; VGCC, voltage-gated

calcium channel; DRG, dorsal root ganglion; EPSC, excitatory postsynaptic current; HP, holding

potential; PNL, partial nerve ligation; PWT, paw withdrawal threshold; RP-HPLC, reversed

phase high performance liquid chromatography; RMSD, root mean squared deviation.

ABSTRACT

N-type Ca^{2+} channel-selective ω-conotoxins have emerged as potential new drugs for the treatment of chronic pain. In this study, two new ω-conotoxins, CVIE and CVIF, were discovered from a *Conus catus* cDNA library. Both conopeptides potently displaced ^{125}I-GVIA binding to rat brain membranes. In *Xenopus* oocytes, CVIE and CVIF potently and selectively inhibited depolarization-activated Ba^{2+} currents through recombinant N-type ($\alpha1_{B-b}/\alpha_2\delta1/\beta_3$) Ca^{2+} channels. Recovery from block increased with membrane hyperpolarization, indicating that CVIE and CVIF have a higher affinity for channels in the inactivated state. The link between inactivation and the reversibility of ω-conotoxin action was investigated by creating molecular diversity in β subunits: N-type channels with β_{2a} subunits almost completely recovered from CVIE or CVIF block, whereas those with β_3 subunits exhibited weak recovery, suggesting that reversibility of the ω-conotoxin block may depend on the type of β subunit isoform. In rat dorsal root ganglion sensory neurons, neither peptide had an effect on (low voltage-activated) T-type channels, but potently and selectively inhibited high voltage-activated N-type Ca^{2+} channels in a voltage-dependent manner. In rat spinal cord slices, both peptides reversibly inhibited excitatory monosynaptic transmission between primary afferents and dorsal horn superficial lamina neurons. Homology models of CVIE and CVIF suggest that ω-conotoxin/voltage-gated Ca^{2+} channel interaction is dominated by ionic/electrostatic interactions. In the rat partial sciatic nerve ligation model of neuropathic pain, CVIE and CVIF (1 nM) significantly reduced allodynic behavior. These N-type Ca^{2+} channel-selective ω-conotoxins are therefore useful as neurophysiological tools and as potential therapeutic agents to inhibit nociceptive pain pathways.

INTRODUCTION

Neuronal (N)-type voltage-gated calcium channels (VGCCs) play important roles in regulating neuronal excitability and nociceptive transmission and are prominently involved in the transduction of acute and chronic pain perception (Snutch, 2005; Yasuda and Adams, 2007). These channels represent important drug targets for the management of chronic and neuropathic pain and have been investigated in the development of new analgesic agents (McGivern, 2006; Schroeder et al., 2006). A number of structurally related ω-conopeptides of the genus *Conus* (cone snails) selectively inhibit N-type VGCCs of pain-sensing primary nociceptors (Olivera et al., 1994). Among these, the ω-conotoxin MVIIA (Ziconotide) still maintains its orphan drug status as a valuable alternative intrathecal analgesic for the management of chronic intractable pain, especially in patients refractory to opioids (Klotz, 2006). Other conopeptides, such as CVID, are currently in clinical trials (McGivern, 2006) and hold promise for the treatment of severe chronic pain in cancer patients. Compared with MVIIA, CVID has a different selectivity profile at N-type calcium channel splice variants and is more selective over P/Q-type calcium channels (Lewis et al., 2000).

The VGCC channel residues that directly interact with ω-conotoxins are not precisely defined, but there is evidence that most of these peptides act at or near the outer vestibule of N-type ($Ca_v2.2$) and P/Q-type ($Ca_v2.1$) VGCCs (Schroeder et al., 2006). However, intracellular domains (Kaneko et al., 2002; McDonough et al., 2002) or auxiliary channel subunits (Lewis et al., 2000; Mould et al., 2004) can also modulate binding kinetics and affinity for the N-type channel. Furthermore, several ω-conotoxins have high affinity for depolarization-inactivated N-type VGCCs, suggesting that channel conformations can be associated with the potency and

reversibility of toxin block (Feng et al., 2003; Stocker et al., 1997).

In vitro, recovery of N-type channels from CVID or MVIIA block is incomplete, whereas GVIA dissociates very slowly from recombinant N-type VGCCs (Mould et al., 2004). CVID, MVIIA and GVIA also cause irreversible inhibition of synaptic transmission between primary afferents and superficial dorsal horn neurons of rats (Motin and Adams, 2008). Conversely, the block by ω-conotoxin CVIB, an antagonist of both N- and P/Q-type VGCCs, has recently been shown to reversibly inhibit excitatory synaptic transmission in the spinal cord (Motin and Adams, 2008). Recovery from block may influence how effectively ω-conotoxins reverse different painful conditions *in vivo*, and could indicate whether administration of these peptides can be controlled to avoid unwanted side effects (Wright et al., 2000).

Conus species have proved a rich source of novel VGCC blockers that have become valuable neurophysiological tools and pain-alleviating therapeutic agents. In the present study, two novel ω-conotoxins (CVIE and CVIF), were discovered following a PCR screen of a cDNA library from the piscivorous cone snail *Conus catus.* We investigated the potency, voltage dependence, and reversibility of synthetic CVIE and CVIF in *Xenopus* oocytes expressing recombinant VGCCs, in isolated sensory neurons dissociated from rat dorsal root ganglia (DRG), and in rat spinal cord slices. CVIE and CVIF displayed voltage-dependent recovery from block and both potently inhibited allodynia associated with the rat partial nerve ligation (PNL) model of chronic pain.

MATERIALS AND METHODS

Gene Isolation and Characterization. *C. catus* venom ducts were emulsified, poly-A$^+$ tailed mRNA extracted using the QuickPrep mRNA purification system (Amersham Pharmacia Biotech, Sydney, Australia), and cDNA libraries produced (Lewis et al., 2000). ω-Conotoxin sequences in the cDNA libararies were then identified using PCR as described previously (Lewis et al., 2000).

Peptide Synthesis. CVIE and CVIF were manually synthesized using Boc *in situ* neutralization solid-phase peptide synthesis (Schnolzer et al., 1992) . Peptides were deprotected and cleaved from the resin as described previously (Schnolzer et al., 1992). Syntheses were carried out on 4-MeBHA-resin. For problematic regions *O*-(7-azabenzotriazol-1-yl)-*N,N,N',N'*-tetramethyluronium hexafluorophosphate was used as a coupling reagent instead of *O*-(benzotriazol-1-yl)-*N,N,N',N'*-tetramethyluronium hexafluorophosphate. Oxidation of the pure reduced peptides (0.05 mM) was achieved using aqueous 0.33 M NH$_4$Oac/0.5 M guanidine HCl (pH 7.8, adjusted with 1 M NH$_4$OH) in the presence of reduced and oxidized glutathione (the molar ratio of peptide:GSH:GSSG was 1:100:10). This solution was stirred at 4°C for 72 hours to produce the folded peptides. Oxidation was monitored using analytical RP-HPLC and mass spectrometry. When oxidation was complete, the pH of the solution was lowered using trifluoroacetic acid (TFA) and the peptides were purified using preparative RP-HPLC.

Peptide Quantitation. Peptides were quantified using RP-HPLC with an external reference standard as described previously (Moffatt et al., 2000). Analyses were performed in triplicate using a Shimadzu 2010 Analytical HPLC system (UV measured at 214 nm) with an Agilent Zorbax C18 column (0.21 x 5 cm, 3.5 μm).

Mass Spectroscopy. Mass spectra were obtained using an Applied Biosystems API2000 LC/MS/MS triple quadrupole mass spectrometer equipped with an ESI source in positive ion mode (m/z 400-1800, with a declustering potential of 10-20V, and 0.1Da steps). The molecular weight of the peptide was deduced from the multiply charged species using Analyst v1.4 with Bioanalyst extensions (Applied Biosystems, Carlsbad, CA). MALDI-TOF MS data were acquired using an Applied Biosystems 4700 MALDI-TOF-TOF proteomics analyzer in reflector positive mode (m/z 500-5000). α-Cyano-4-hydroxy cinnamic acid (10mg/ml) was used as the matrix solution.

HPLC Analysis. Analytical RP-HPLC was performed on a Shimadzu HPLC system using a Vydac C18 column (0.46 x 25 cm, 5 μm). Separation was achieved using a linear gradient increasing at 1% solvent B/min with a flow rate of 1ml/min over 35 mins. Preparative RP-HPLC was performed on a Waters HPLC system using a Vydac C18 column (2.2 x 25 cm, 10 μm). A linear gradient over 35 min was used, increasing at 1% solvent B/min at a flow rate of 10 ml/min. Solvent A was 0.05% aqueous TFA, solvent B was 90% acetonitrile/H_2O with 0.43% TFA.

^{125}I-GVIA Binding Assay. The affinity of GVIA, CVID, CVIE, and CVIF at N-type VGCCs was determined from displacement of ^{125}I-GVIA binding to rat brain membranes, as described previously (Lewis et al., 2000).

Complementary DNA clones of Ca^{2+} channel subunits. Clones of rat $Ca_v2.2$ α_{1B-b} (N-type, peripheral isoform), rat $Ca_v1.3$ α_{1D} (L-type), and rat ß$_3$ cDNAs were provided by Dr. D. Lipscombe (Brown University, Providence, RI); rabbit $Ca_v1.2$ α_{1C} (L-type), rabbit $Ca_v2.1$ α_{1A} (P/Q-type), rat $Ca_v2.3$ α_{1E} (R-type), and rat ß$_{2a}$ cDNAs were provided by Dr. G. Zamponi

(University of Calgary, Calgary, Canada). Rabbit $\alpha_2\delta1$ cDNA was provided by Dr. F. Hofmann and Dr. N. Klugbauer (Technische Universität München, Germany).

***Xenopus* Oocyte Injection and Electrophysiology.** All animal experimentation in this study was performed in accordance with the U.S. National Institutes of Health guidelines and was approved by the University of Queensland and University of Sydney Animal Ethics Committees. Stage V–VI oocytes from *Xenopus laevis* frogs were surgically removed and cultured as described previously (Yasuda et al., 2004). Capped RNA transcripts encoding full-length VGCC pore-forming and auxiliary subunits were synthesized using the mMessage mMachine *in vitro* transcription kit (Ambion, Applied Biosystems). For recombinant N- ($Ca_v2.2$) or L-type ($Ca_v1.2$ or $Ca_v1.3$) VGCC expression, the oocytes were injected with 50 nl of solution containing a mixture of cRNAs encoding either α_{1B-b} subunit (5 ng/cell) or α_{1C} subunit (5 ng/cell), or α_{1D} subunit (5 ng/cell), and $\beta3$ subunit (8 or 12 ng/cell) with or without $\alpha_2\delta1$ subunit (5 ng/cell). For $\alpha_{1B-b}/\alpha_2\delta1/\beta_{2a}$ VGCC expression, 0.5 ng/cell β_{2a} subunit cRNA was used. For recombinant expression of P/Q- or R-type VGCCs, the oocyte nucleus was first injected with 9 nl of cDNA encoding for $Ca_v2.1$ α_{1A} (4.5 ng/cell) or $Ca_v2.3$ α_{1E} (4.5 ng/cell) subunits, respectively, after which the cytoplasm was injected with cRNAs encoding auxiliary subunits. Following injection, oocytes were kept at 18 °C for 3–7 days for recombinant calcium channel expression, as described previously (Yasuda et al., 2004). Depolarization-activated Ba^{2+} or Ca^{2+} currents (I_{Ba} and I_{Ca}, respectively) were recorded using a two-electrode virtual ground voltage-clamp circuit with a GeneClamp 500B amplifier controlled by a Clampex9.2/DigiData1332 acquisition system (Molecular Devices, Sunnyvale, CA). Prior to recording, oocytes were injected with 30 nl of 50 mM BAPTA to eliminate endogenous Ca^{2+}-activated Cl^- conductance. The oocytes were placed in a 0.1 ml recording chamber and superfused at a constant rate of 3

ml/min. The external bath solution contained (in mM): 5 $BaCl_2$, 85 tetraethylammonium hydroxide (TEA-OH), 5 KCl, 10 HEPES, pH 7.4 (with methanesulfonic acid). In a series of experiments, 5 mM $BaCl_2$ was substituted by 5 mM $CaCl_2$ in the external bath solution. Borosilicate glass microelectrodes were filled with 3 M KCl and had resistances of 0.4–1.2 MΩ. Oocytes were voltage-clamped at various holding potentials, and membrane currents were elicited by 200 ms step depolarizations to 0 mV ($Ca_V2.2$ and $Ca_v1.2$), +10 mV ($Ca_V2.1$), +10 mV ($Ca_V2.3$), or –30 mV ($Ca_V1.3$), applied every 10 s. Experiments were only commenced when the alteration of peak current evoked by repeated depolarizing pulses was reduced to less than ±2% within a 1-min period (Yasuda et al., 2004). Leak and capacitive currents were subtracted using a −P/4 pulse protocol and current amplitudes were monitored on-line using the Clampex 9.2 software package. Currents were filtered at 1 or 2 kHz, digitized at 5 kHz and stored on a computer hard-drive.

Primary Culture of DRG Neurons and Patch-Clamp Recording. DRG neurons were enzymatically dissociated from ganglia of 7–14 day-old Wistar rats, as described previously (Motin et al., 2007) and used for experiments within 24–48 h. Cells were transferred into a small-volume (~200 µl) recording chamber constantly perfused with a solution containing (in mM): 150 tetraethylammonium chloride (TEA-Cl), 2 $BaCl_2$, 10 D-glucose, 10 HEPES, pH 7.4 (with NaOH). Borosilicate glass electrodes were filled with an internal solution containing (in mM): 140 CsCl, 1 $MgCl_2$, 5 MgATP, 0.1 Na-GTP, 5 BAPTA-Cs_4, 10 HEPES, pH 7.3 (with CsOH) and had resistances of 1.5-2.5 MΩ. Patch-clamp recordings were performed with a Multiclamp 700B amplifier controlled by Clampex9.2/DigiData1332 acquisition system (Molecular Devices), at room temperature (23–25°C). Unless indicated otherwise, whole-cell I_{Ba} was elicited by 200 ms step depolarizations to 0 mV, applied every 15 s, from a holding potential

of −80 mV, in the voltage-clamp configuration of the patch-clamp technique. Currents were filtered at 2 kHz and sampled at 5 kHz. Leak and capacitative currents were subtracted using a −P/4 pulse protocol. Data were stored digitally on a computer for further analysis.

Spinal Cord Slice Preparation. The spinal cord was isolated from 8–15 day-old Wistar rats as previously described (Motin and Adams, 2008). Before experiments, slices were kept in artificial cerebrospinal fluid for 1 h at 37° C. In spinal cord slices, lamina I–II neurons of the rat superficial dorsal horn were located using an infrared camera. Patch-clamp borosilicate glass electrodes (Harvard Apparatus Ltd., Edenbridge, UK) were filled with a solution containing (in mM): 130 KF, 10 KCl, 10 EGTA, 1 $MgCl_2$, and 10 HEPES (pH 7.2 with KOH), resulting in resistances of 1.5–3 MΩ. The calculated liquid junction potential of 6.4 mV was not compensated. Upon formation of whole-cell recording configuration, neurons were first held in current-clamp configuration to evaluate their resting membrane potential and responses to depolarizing current injections. Excitatory postsynaptic currents (EPSCs) were recorded under voltage-clamp conditions, from a holding potential of -80 mV, in the presence of 100 μM picrotoxin and 10 μM strychnine to block inhibitory synaptic transmission, and were categorized as monosynaptic or polysynaptic responses, as described previously (Motin and Adams, 2008). EPSC amplitude was monitored on-line using Clampex 9.2 software package. Data were filtered at 10 kHz, digitized at 50 kHz and stored on a computer for further analysis. Off-line analysis was performed using custom-written software in MATLAB (The Mathworks Inc., Natick, MA), as described previously (Motin and Adams, 2008).

Intrathecal CVIE and CVIF in Neuropathic Pain. Experiments were performed on 24 male Sprague-Dawley rats weighing 200–260 g. Rats were housed four per cage and were maintained on a standard 12-h light/dark cycle with free access to food and water. Rats

underwent partial ligation of the left sciatic nerve (PNL), as described previously (Ekberg et al., 2006). In rats that developed significant mechanical allodynia 7 days after surgery, chronic polyethylene lumbar intrathecal catheters were inserted between vertebrae L5 and L6, advanced 3 cm rostrally and exteriorized via the occipital region. All of these procedures were carried out under isoflurane anesthesia. Intrathecal injections were made via the exteriorized catheter 10-12 days after PNL surgery using gentle restraint. Peptides were dissolved in 0.9% saline to the desired concentration on the day of the experiment and were injected in a volume of 10 μl, followed by 15 μl of 0.9% saline to wash the drug from the catheter dead-space. Control animals received injections of the corresponding vehicle. Mechanical paw withdrawal threshold (PWT) was measured with a series of von Frey hairs (range 0.4–15 g) using the up-down paradigm (Chaplan et al., 1994), as described previously (Ekberg et al., 2006). The maximum possible score (15 g) was recorded when animals failed to respond to the 15 g von Frey hair. Pre-surgery baseline thresholds were 14.7 ± 0.3 g (n = 21). The experimenter was blinded to all drug treatments. Catheter patency and placement were confirmed after all experiments by postmortem visualization of the spread of a second intrathecal methylene blue injection (10 ml, 4%) over the lumbar enlargement.

Molecular Modeling. Molecular models of ω-conotoxins CVIE and CVIF were built in the program *Modeller 9v2* using MVIIA (PDB ID 1TTK (Adams et al., 2003) as the template since they share a high degree of protein sequence identity (~80%). The sequence alignment was generated using *ClustalW* (Larkin et al., 2007). Models that disagreed with the known intramolecular interactions were excluded. The energy minimization of the ω-conotoxin models was performed using the program *GROMOS* (Scott et al., 1999). All 3D structure representations were prepared using the program *Pymol* (DeLano Scientific LLC, Palo Alto, CA).

Chemicals and Drugs. Boc-L-amino acids were purchased from Merck (Darmstadt, Germany) and the Peptide Institute (Osaka, Japan). 4-meBHA resin was from the Peptide Institute. *O*-(Benzotriazol-1-yl)-*N,N,N',N'*-tetramethyluronium hexafluorophosphate and reduced and oxidized glutathione were from Sigma-Aldrich Pty Ltd (Sydney, Australia). *O*-(7-Azabenzotriazol-1-yl)-*N,N,N',N'*-tetramethyluronium hexafluorophosphate was from Genscript (Piscataway, NJ). Dichloromethane and NH_4Oac were from Merck. *N,N*-diisopropylethylamine, *N,N*-dimethylformamide and trifluoroacetic acid (TFA) were from Auspep (Melbourne, Australia). Guanidine HCl was from Amresco (Solon, USA). Other reagents and solvents were analytical reagent grade. ω-Conotoxin CVIB was prepared as described previously (Lewis et al., 2000), ω-Agatoxin IVA was purchased from the Peptide Institute. Nifedipine (Sigma) was freshly prepared from a stock solution in ethanol. Various drugs and toxins were diluted to the final concentration immediately before the experiment and bath applied.

Curve Fitting and Statistical Analysis. Concentration-response curves were obtained by plotting averaged relative peak current amplitude values (I/I_0) *vs.* toxin concentration and fitting the resulting data by the Hill equation $I = I_0\{[CTX]^n/(IC_{50}^n + [CTX]^n)\}$, where I_0 is the maximum peak current amplitude, [CTX] the conotoxin concentration, *n* the Hill coefficient, and IC_{50} the agonist concentration that produces 50% of the maximum response; pIC_{50} values were defined as $-\log IC_{50}$. The blocked fraction was determined as I/I_0, while the recovered fraction was defined as $[(I_{rec}-I)/(I_0-I)]$, where I_0 is the maximum peak current amplitude, I the blocked current amplitude, and I_{rec} the current amplitude after washout.

Data are mean $\pm$ SEM (n, number of experiments). Statistical analyses were performed using the Student's *t*-test for two groups, and one-way ANOVA or two-way ANOVA for multiple comparisons; differences were considered significant if $p < 0.05$.

RESULTS

PCR amplification and synthesis of CVIE and CVIF from *Conus catus*. PCR of the *C. catus* venom duct cDNA templates resulted in a DNA product of approximately 380-500 bp (data not shown). Two PCR products that translated to putative mature peptides were named CVIE and CVIF. The predicted amino acid sequences derived for CVIE and CVIF are shown in Table I, and are aligned with the sequences of related ω-conotoxins. Homology screening of public nucleotide and amino acid databases with the CVIE and CVIF sequences indicated that both sequences were unique.

Radioligand binding. Synthetic CVIE and CVIF fully displaced ^{125}I-GVIA binding to rat brain membrane. Despite the structural variations, affinities of CVIE (25 pM) and CVIF (98 pM) were not significantly different from those of GVIA and CVID (Fig. 1).

CVIE and CVIF are selective inhibitors of recombinant N-type VGCCs. ω–Conotoxins CVIE and CVIF (0.1-3 μM) potently inhibited depolarization-activated Ba^{2+} currents (I_{Ba}) through $Ca_v2.2$ channels expressed in *Xenopus* oocytes (Fig. 2A). At the highest concentration tested (3 μM), neither peptide had any effect on recombinant $Ca_v1.2$, $Ca_v1.3$, or $Ca_v2.3$ channels (n ≥ 5 in all cases) assembled from pore-forming α and auxiliary $α_2δ1$ and $β_3$ subunits (not shown). However, 3 μM CVIE or CVIF caused a minor (< 10%) inhibition of $Ca_v2.1$ ($α/α_2δ1/β_3$) channels (n ≥ 5). We recorded I_{Ba} in the absence and presence of a single concentration (100 nM) of ω-conotoxin CVIE, CVIF or CVIB for comparison (Fig. 2B). In a series of experiments, we investigated the influence of the $α_2δ1$ auxiliary subunit on the pharmacological profile of CVIE or CVIF block, and applied increasing concentrations of ω-conotoxin to produce cumulative concentration-response relationships (Fig. 2B). These relations were described by Hill equations

with IC_{50} and Hill slope values of 2.6 ± 0.5 nM and 0.45 ± 0.03 (n = 14) for CVIE, 19.9 ± 3.2

nM and 0.51 ± 0.04 (n = 16) for CVIF, and 12.0 ± 2.3 nM and 0.47 ± 0.03 (n = 8) for CVIB,

respectively. In the absence of $\alpha_2\delta1$, the following IC_{50} and Hill slope values were obtained: 0.12

± 0.05 nM and 0.36 ± 0.04 (n = 6) for CVIE, 0.1 ± 0.07 nM and 0.26 ± 0.04 (n = 7) for CVIF,

and 1.6 ± 0.6 nM and 0.41 ± 0.04 (n = 5) for CVIB, respectively. N-type Ca^{2+} channel inhibition

by any of the above ω-conotoxins was ~10-20 fold more potent in the absence of the $\alpha_2\delta1$

auxiliary subunit compared to that observed in the presence of $\alpha_2\delta1$, confirming our previous

results (Mould et al., 2004).

N-type VGCC recovery from CVIE or CVIF block is voltage dependent. For a series of

ω-conotoxins (e.g. GVIA, MVIIA, and MVIIC), the amount of N-type Ca^{2+} channel block and

the current fraction recovered, as well as the kinetics of onset and recovery from toxin block,

have been shown to be affected by the holding potential (HP) (Feng et al., 2003; Stocker et al.,

1997). We first assessed recombinant $(\alpha_{1B-b}/\alpha_2\delta_1/\beta_3)$ N-type VGCC availability from HPs of –80

or –125 mV, in the absence of ω-conotoxin (Fig. 3A). Consistent with our previous results

(Yasuda et al., 2004), these N-type channels exhibited robust inactivation at a HP of –80 mV.

However, channels rapidly became available when the HP was changed from –80 mV to –125

mV, and inactivated when the membrane potential was returned to –80 mV, following time

courses which could be best described by the sum of two exponential functions (Yasuda et al.,

2004). At this voltage, when the peak I_{Ba} approached quasi steady-state amplitude, 100 nM CVIF

or CVIE (n = 2; not shown) was applied until complete block developed, after which the toxin

was washed off. Recovery from ω-conotoxin block was strongly affected by the HP: at –80 mV,

recovery was slow and incomplete (Fig. 3A, asterisk), but upon return to –125 mV the current

fully recovered to its pre-toxin, hyperpolarized –125 mV HP level. In these experiments often

exceeding 40-50 min duration, run-down of the I_{Ba} could occur and, despite BAPTA injection, endogenous (background) currents could develop. To minimize these currents, we recorded I_{Ba} from oocytes with relatively low Ca^{2+} channel expression levels (36-48 h after injection), and limited the inactivation-recovery time (from a to b; Fig. 3A) and inactivation time (from b to c; Fig. 3A), therefore, complete recovery or maximum inactivation, respectively, was only approached. This, however, did not significantly affect the outcome of the experiment. To gain further insight into the mechanism of voltage-dependent ω-conotoxin block, the fractions of currents blocked and recovered at various HPs were examined following application and washout of each peptide, in the voltage range between –65 and –125 mV. In general, the HP had statistically non-significant effects on the fraction blocked; however the HP markedly determined the fraction of current recovery from block (Fig. 3B). For example, at –65 mV HP, the current recovered only partially from CVIF block (20.3 ± 3.9 %, n = 4), whereas at –125 mV the recovery was almost complete (99 ± 4 %, n = 3). Similarly, in the absence of the $\alpha_2\delta1$ subunit, the recovery from CVIE or CVIF block was voltage dependent, which persisted upon replacement of Ba^{2+} as the charge carrier with the physiological ion, Ca^{2+} (not shown). Data demonstrating that recovery from ω-conotoxin block is favored at strong membrane hyperpolarization are qualitatively consistent with those of Stocker et al. (Stocker et al., 1997) and suggest that CVIE and CVIF have higher affinity for the inactivated state of the N-type Ca^{2+} channels. In contrast, recovery of recombinant N-type VGCCs from CVIB block does not exhibit voltage dependence (Fig. 3B). Voltage-dependent control of CVIE and CVIF displacement could be useful in experiments in which reversibility of blockade of N-type VGCCs is important (Stocker et al., 1997), allowing peptide toxins to be locked to or released from the site of interaction depending on the gating state of the channel.

Auxiliary β subunits modulate recovery from CVIE and CVIF block. We further investigated the link between N-type VGCC inactivation and the reversibility of ω-conotoxin action by creating molecular diversity in the β subunits, resulting in VGCCs with a fast ($\alpha1_{B-b}/\alpha_2\delta1/\beta_3$) or profoundly slow ($\alpha1_{B-b}/\alpha_2\delta1/\beta_{2a}$) time course of inactivation. At a HP of –80 mV, VGCCs with β_{2a} subunits almost recovered completely from CVIE or CVIF block (Figs. 4A and 4C), whereas VGCCs with β_3 subunits exhibited relatively weak recovery (Figs. 3B, 4B-C). The HP did not affect recovery of N-type channels with β_{2a} subunits from CVIE or CVIF block, as complete recovery was also obtained at –125 mV (n = 3, data not shown).

We also tested ω-conotoxins closely related to CVIE and CVIF: GVIA, previously shown to exhibit weak voltage-dependent reversibility compared to CVIE or CVIF, and CVIB, shown to lack voltage-dependent reversibility. Remarkably, recovery from GVIA block also appeared to be β subunit-dependent (Fig. 4C). However, the I_{Ba} fraction recovered from CVIB block was not affected by auxiliary β subunits (Figs. 3B, 4A-C).

CVIE and CVIF selectively inhibit native N-type VGCCs in DRG neurons. To assess any differences in pharmacology at native *versus* cloned VGCCs, the selectivity and reversibility of these novel ω-conotoxins was evaluated at native N-type VGCCs in acutely dissociated DRG sensory neurons (Fig. 5). Both CVIE and CVIF (100 nM) inhibited whole-cell Ba^{2+} currents through VGCCs, and the recovery from block was voltage dependent (Figs. 5A-C). The maximum inhibition of inward Ba^{2+} current produced by 100 nM CVIE or CVIF in DRG neurons was ~50 % (Fig. 5B), which is similar to that reported previously for N-type selective ω-conotoxins CVID, MVIIA, or GVIA (Motin et al., 2007). The residual I_{Ba} in the presence of these ω-conotoxins (1 μM) represents non-N-type current through other (mostly L-, P/Q-, and R-type) VGCCs, which can be selectively inhibited (Motin et al., 2007). Bath application of CVIB

(500 nM) and nifedipine (10 μM) to inhibit P/Q- and L-type VGCC currents, respectively, demonstrated that neither CVIE nor CVIF affected these current components (Fig. 5D). In two cases, 100 nM of ω-agatoxin-IVA was used instead of CVIB, producing the same effect (not shown). In 21% of cells studied (15/70), a low-voltage-activated T-type VGCC was identified using depolarizing voltage steps negative to –40 mV (i.e. weak depolarizations above HP). However, at the highest concentration tested (1 μM), these channels were not affected by either ω-conotoxin CVIE (n = 3) or CVIF (n = 4) (Fig. 5E).

CVIE and CVIF inhibit excitatory synaptic transmission in rat spinal cord. Multiple types of presynaptic VGCCs contribute to neurotransmitter release at peripheral and central synapses (Engelman and MacDermott, 2004). Our experimental model mimics the propagation of a nociceptive signal along primary afferents following the electrical stimulation of the dorsal root. Recordings were made from neurons confined within the *substantia gelatinosa* - the region where Aδ- and C-fibers primarily terminate. The effects of the ω-conotoxins CVIE (100 nM) and CVIF (100 nM) were examined on the excitatory synaptic transmission between primary afferents and dorsal horn superficial lamina neurons, a process predominantly (Heinke et al., 2004), if not entirely (Motin and Adams, 2008), controlled by N-type VGCCs. CVIE and CVIF reversibly reduced evoked monosynaptic EPSC amplitude by an average of 67 ± 5 % (n = 7) and 61 ± 7 % (n = 6), respectively, compared to control. The EPSC amplitude recovered to 78 ± 7% and 73 ± 10% of control 10–15 min after block by CVIE (n = 6) and CVIF (n = 5), respectively (Fig. 6).

Intrathecal CVIE and CVIF blocks chronic pain behavior in a rat model of persistent pain. PNL produced a profound reduction in paw withdrawal threshold from the pre-surgery baseline of 14.7 ± 0.3 g (n = 21), indicating the development of mechanical allodynia (Fig. 7). As

17

reported previously for CVID (Scott et al., 2002), a dose of 1 nM of intrathecal CVID, CVIE or CVIF produced significant reversal of mechanical allodynia to pre-injury baseline levels (two-way ANOVA, $p < 0.001$). Each peptide produced side effects typical of ω-conotoxins, including shakes and tail twitching and serpentine tail movements, as reported previously for CVID (Scott et al., 2002).

Homology models of ω-conotoxins CVIE and CVIF. In order to provide initial molecular insights into the differences in pharmacology amongst ω-conotoxins, we generated a homology model of CVIE and CVIF using MVIIA as the structural template. Comparison of CVIE, CVIF, MVIIA and MVIIC structures revealed a conserved positively charged cluster on one side of the molecule and a mainly neutral surface on the opposite face (Fig. 8).

Another interesting finding was that the hydrophobic patches of these ω-conotoxins were randomly distributed throughout the molecule (data not shown), suggesting that ω-conotoxin VGCC interaction is dominated by ionic/electrostatic interactions. In addition, a very similar structural fold for the postulated pharmacophore (position 10, 11 and 13) of CVIE, CVIF, MVIIA and MVIIC was observed (Fig. 9). The most significant difference between the pharmacophore of the four ω-conotoxins was at position 10, where it differs by one methyl group in length, whereas the Y13 of all four ω-conotoxins are orientated similarly (RMSD < 0.5Å).

DISCUSSION

N-type VGCC selective ω-conotoxins are a new class of therapeutics for the treatment of chronic and neuropathic pain (Schroeder et al., 2006). In this study, we characterized two novel ω-conotoxins that discriminate between N-type and other types of VGCCs found in normal and chronic pain pathways.

CVIE and CVIF were discovered using a PCR approach enabling minor conopeptides – which are difficult to isolate from crude venoms to be identified and sequenced. Both peptides showed a high degree of sequence homology to other *Conus catus* ω-conopeptides with a 6-cysteine/4-loop consensus framework (Table I) and, in binding assays, exhibited similar affinities for rat brain VGCCs as do GVIA and CVID.

In *Xenopus* oocytes, CVIE and CVIF potently and selectively inhibited Ba^{2+} currents through recombinant N-type ($\alpha_{1B-b}/\alpha_2\delta1/\beta_3$) channels. These channels have a hyperpolarized voltage-dependent inactivation range compared to other types of VGCCs (Nowycky et al., 1985). Under our experimental conditions, approximately half of the recombinant N-type channels were inactivated at a HP of –85 mV, due to a β_3 subunit-mediated effect on the inactivation (Canti et al., 2001; Yasuda et al., 2004). The voltage dependence of CVIE, CVIF and CVIB block and recovery was determined by carrying out experiments at various HP values. The HP had an insignificant effect on the efficacy of CVIE and CVIF block of I_{Ba}, whereas membrane hyperpolarization facilitated recovery from CVIE and CVIF block. These findings suggested a correlation between the degree of channel inactivation and the change of toxin-blocking characteristics: CVIE and CVIF had higher affinity for channels in the inactivated state and strong hyperpolarization alleviated toxin association with the channel. This was also evident in

19

experiments during which the HP was switched within the experiment following the application

of CVIE or CVIF (see Fig 3A). Next, we investigated the effect of the β_{2a} subunit (Fig. 4),

demonstrating that recovery from CVIE and CVIF block depends on the auxiliary β subunit

isoform, and therefore linking N-type VGCC inactivation and reversibility. However, the

molecular mechanism linking CVIE or CVIF recovery and Ca^{2+} channel inactivation remains to

be determined. Recent data have elegantly shown that the β_{2a} subunit slows channel inactivation

by restricting the movement of the IS6 pore-lining segment of the α_1 subunit (Van Petegem et

al., 2004), perhaps resulting in a conformation that facilitates unbinding of these peptide toxins.

Block of N-type VGCCs by various ω-conotoxins can differ substantially. For example, in

the presence of SNX-331, a derivative of MVIIC, not only recovery from block (fraction

recovered), but also the amount of block (I/I_0) exhibits strong voltage dependence, whereas for a

number of other ω-conotoxins (e.g. GVIA, MVIIC, MVIIA and TVIA), the voltage dependence

of block is weaker compared to that of SNX-331 (Stocker et al., 1997). A detailed analysis of the

effect of MVIIA on the N-type channel confirmed that block was neither voltage-, nor

frequency-dependent, but recovery from block strongly depended on the HP (Feng et al., 2003).

In contrast, our previous studies of ω-conotoxin CVID demonstrated that hyperpolarization does

not significantly enhance the extent of recovery (Mould et al., 2004); CVIB block and recovery

also appeared to be largely voltage independent (Motin et al., 2007). Although the degree of N-

type channel inactivation appears to be a key factor modulating the ω-conotoxin ion channel

binding site interaction, several unknown mechanisms also contribute in determining the relative

proportion of reversibly and irreversibly blocked channels (Feng et al., 2003). We did not

conduct experiments to assess CVIE and CVIF block in various (e.g. open, inactivated or

resting) states, but rather assume that their potencies to block N-type VGCCs are state

independent, similar to that of MVIIA (Feng et al., 2003).

There is evidence for specific expression of VGCC variants in defined pain pathways, which could represent novel targets for pain management. For example, the exon 37a splice isoform of Cav2.2 α_{1B} is expressed preferentially in capsaicin-responsive neurons (Bell et al., 2004), and is specifically required for mediating basal thermal nociception, as well as for developing thermal and mechanical hyperalgesia during inflammatory and neuropathic pain (Altier et al., 2007). One recently identified feature of neuropathic pain is the upregulation of the $\alpha_2\delta1$ subunit that associates with VGCCs in DRGs (Luo et al., 2001; Newton et al., 2001). This is of particular significance as the potency of MVIIA and CVID at the N-type VGCC (α_{1B-b} and α_{1B-d}) is largely reduced by co-expression with $\alpha_2\delta1$ (Mould et al., 2004). CVIE and CVIF exhibited a somewhat lower, ~10- to 20-fold decrease in potency in the presence of $\alpha_2\delta1$ (Fig. 3). N-type VGCCs control nerve-evoked neurotransmitter release and are associated with nociceptive synaptic transmission (Kerr et al., 1988). Blocking VGCCs in both DRG cell bodies and their synaptic terminals in the spinal cord dorsal horn reduces the release of glutamate and neuropeptides (e.g. substance P and calcitonin gene-related peptide) (Snutch, 2005), and leads to a reduced sensation of various noxious painful stimuli. In acutely isolated DRG neurons, the selectivity and voltage-dependent effects of CVIE and CVIF were qualitatively similar to those observed for heterologously expressed N-type channels. Furthermore, low-voltage-activated T-type Ca^{2+} channels, which have pro-nociceptive roles in acute and chronic pain states (Altier and Zamponi, 2004), were not inhibited by either CVIE or CVIF.

Recently, we have shown that inhibition of excitatory monosynaptic transmission by a series of N-type VGCC-selective ω-conotoxins is largely irreversible (Motin and Adams, 2008). In contrast, in the present study CVIE and CVIF inhibition of excitatory synaptic transmission was

reversible (Fig. 6). The reason for this effect is unclear, but is likely to be due to the presence of an inactivation-resistant N-type Ca^{2+} channel population in the presynaptic nerve terminals, especially as the bulk of presynaptic N-type VGCCs are resistant to voltage-dependent inactivation (Stanley, 2003). These channels are also subject to modulation by release site-associated proteins (Stanley, 2003) and by subunit-specific dynamic palmitoylation (Hurley et al., 2000). Our results demonstrate that β subunits are likely to play important roles in determining reversibility of ω-conotoxin block. This is important, considering that β_{1-4} subunits and their splice variants have different expression levels in various tissues (Dolphin, 2003).

ω-Conotoxins, including CVID, have consistently been reported to alleviate neuropathic pain following intrathecal administration in rodent models (Scott et al., 2002). The present study has established that CVIE and CVIF similarly reverse signs of neuropathic pain (allodynia) in the PNL model. CVID, CVIE and CVIF all produced side effects similar to those reported previously for ω-conotoxins (Scott et al., 2002). Generally, ω-conotoxins have demonstrated efficacy, but have a relatively low therapeutic index (TI). A number of these peptides selectively inhibit presynaptic N-type channel activity, and hence, disrupt pain signals. Chemical modifications of ω-conotoxins can lead to improved biopharmaceutical properties and guide the rational development of specific N-subtype VGCC inhibitors (Schroeder et al., 2006). Future advances should also come with the discovery of new molecules, including novel conopeptides, which are more selective for pain pathways and analgesia modalities.

Future experiments should clarify whether the R10K analogs of CVIE and CVIF exhibit altered potency, voltage dependence, and/or reversibility during the block of recombinant or native N-type VGCCs and synaptic transmission.

Comparing our homology models to the structures of MVIIA and MVIIC revealed a conserved and distinctive charge distribution. The highly conserved Y13 on the neutral side of the ω-conotoxins is oriented in an almost identical manner, consistent with it playing a key role in binding to N-type VGCCs (Adams et al., 2003; Nielsen et al., 2000), presumably through a hydrogen bond from the hydroxyl group on Y13 to the channel. Secondly, the positively charged face of ω-conotoxins is mostly distributed across loop2 and loop4 residues, and is to likely contribute to VGCC binding via ionic and/or electrostatic interactions. However, due to the low sequence conservation across this region, these interactions may help orient ω-conotoxins during binding. This is consistent with the previous structure-activity relationship studies, where at least four residues in addition to Y13 (mostly positively charged residues) from loop2 and loop4 were found to contribute to N-type VGCC affinity (Nadasdi et al., 1995; Nielsen et al., 2000). Furthermore, the sequence analysis of ω-conotoxins reveals a highly conserved positively charged patch at position 10, a position previously shown to affect VGCC selectivity and voltage-dependent recovery from block (Adams et al., 2003). It appears that subtle changes in side-chain length can influence how ω-conotoxins interact with N-type VGCCs, with *C. catus* evolving ω-conotoxins utilizing both R10 (CVIA, CVIE, CVIF) and K10 (CVIB, CVID).

In summary, the ω-conotoxins CVIE and CVIF are potent, selective and reversible N-type VGCC blockers, potentially useful neurophysiological tools and potent inhibitors of nociceptive signaling. For the first time, we demonstrate, that N-type calcium channel recovery from ω-conotoxin block can depend on the type of β subunit isoform and provide a direct demonstration of the role of calcium channel inactivation in ω-conotoxin action. It remains to be seen whether ω-conotoxins that have a more favorable ratio of anti-nociception to side effects profile than Prialt (MVIIA) and AM336 (CVID) can be uncovered.

MOL #58834

REFERENCES

Adams DJ, Smith AB, Schroeder CI, Yasuda T and Lewis RJ (2003) ω-Conotoxin CVID inhibits a pharmacologically distinct voltage-sensitive calcium channel associated with transmitter release from preganglionic nerve terminals. *J Biol Chem* **278:** 4057-4062.

Altier C, Dale CS, Kisilevsky AE, Chapman K, Castiglioni AJ, Matthews EA, Evans RM, Dickenson AH, Lipscombe D, Vergnolle N and Zamponi GW (2007) Differential role of N-type calcium channel splice isoforms in pain. *J Neurosci* **27:** 6363-6373.

Altier C and Zamponi GW (2004) Targeting Ca^{2+} channels to treat pain: T-type versus N-type. *Trends Pharmacol Sci* **25:** 465-470.

Bell TJ, Thaler C, Castiglioni AJ, Helton TD and Lipscombe D (2004) Cell-specific alternative splicing increases calcium channel current density in the pain pathway. *Neuron* **41:** 127-138.

Canti C, Davies A, Berrow NS, Butcher AJ, Page KM and Dolphin AC (2001) Evidence for two concentration-dependent processes for β-subunit effects on α_{1B} calcium channels. *Biophys J* **81:** 1439-1451.

Chaplan SR, Bach FW, Pogrel JW, Chung JM and Yaksh TL (1994) Quantitative assessment of tactile allodynia in the rat paw. *J Neurosci Methods* **53:** 55-63.

Dolphin AC (2003) β Subunits of voltage-gated calcium channels. *J Bioenerg Biomembr* **35:** 599-620.

Ekberg J, Jayamanne A, Vaughan CW, Aslan S, Thomas L, Mould J, Drinkwater R, Baker MD, Abrahamsen B, Wood JN, Adams DJ, Christie MJ and Lewis RJ (2006) μO-conotoxin

MOL #58834

MrVIB selectively blocks Nav1.8 sensory neuron specific sodium channels and chronic pain behavior without motor deficits. *Proc Natl Acad Sci U S A* **103:** 17030-17035.

Engelman HS and MacDermott AB (2004) Presynaptic ionotropic receptors and control of transmitter release. *Nat Rev Neurosci* **5:** 135-145.

Feng ZP, Doering CJ, Winkfein RJ, Beedle AM, Spafford JD and Zamponi GW (2003) Determinants of inhibition of transiently expressed voltage-gated calcium channels by ω-conotoxins GVIA and MVIIA. *J Biol Chem* **278:** 20171-20178.

Heinke B, Balzer E and Sandkuhler J (2004) Pre- and postsynaptic contributions of voltage-dependent Ca^{2+} channels to nociceptive transmission in rat spinal lamina I neurons. *Eur J Neurosci* **19:** 103-111.

Hurley JH, Cahill AL, Currie KP and Fox AP (2000) The role of dynamic palmitoylation in Ca^{2+} channel inactivation. *Proc Natl Acad Sci U S A* **97:** 9293-9298.

Kaneko S, Cooper CB, Nishioka N, Yamasaki H, Suzuki A, Jarvis SE, Akaike A, Satoh M and Zamponi GW (2002) Identification and characterization of novel human $Ca_v2.2$ (α_{1B}) calcium channel variants lacking the synaptic protein interaction site. *J Neurosci* **22:** 82-92.

Kerr LM, Filloux F, Olivera BM, Jackson H and Wamsley JK (1988) Autoradiographic localization of calcium channels with [^{125}I]ω-conotoxin in rat brain. *Eur J Pharmacol* **146:** 181-183.

Klotz U (2006) Ziconotide--a novel neuron-specific calcium channel blocker for the intrathecal treatment of severe chronic pain--a short review. *Int J Clin Pharmacol Ther* **44:** 478-483.

Larkin MA, Blackshields G, Brown NP, Chenna R, McGettigan PA, McWilliam H, Valentin F, Wallace IM, Wilm A, Lopez R, Thompson JD, Gibson TJ and Higgins DG (2007) Clustal W and Clustal X version 2.0. *Bioinformatics* **23:** 2947-2948.

Lewis RJ, Nielsen KJ, Craik DJ, Loughnan ML, Adams DA, Sharpe IA, Luchian T, Adams DJ, Bond T, Thomas L, Jones A, Matheson JL, Drinkwater R, Andrews PR and Alewood PF (2000) Novel ω-conotoxins from *Conus catus* discriminate among neuronal calcium channel subtypes. *J Biol Chem* **275:** 35335-35344.

Luo ZD, Chaplan SR, Higuera ES, Sorkin LS, Stauderman KA, Williams ME and Yaksh TL (2001) Upregulation of dorsal root ganglion $\alpha_2\delta$ calcium channel subunit and its correlation with allodynia in spinal nerve-injured rats. *J Neurosci* **21:** 1868-1875.

McDonough SI, Boland LM, Mintz IM and Bean BP (2002) Interactions among toxins that inhibit N-type and P-type calcium channels. *J Gen Physiol* **119:** 313-328.

McGivern JG (2006) Targeting N-type and T-type calcium channels for the treatment of pain. *Drug Discov Today* **11:** 245-253.

Moffatt F, Senkans P and Ricketts D (2000) Approaches towards the quantitative analysis of peptides and proteins by reversed-phase high-performance liquid chromatography in the absence of a pure reference sample. *J Chromatogr A* **891:** 235-242.

Motin L and Adams DJ (2008) ω-Conotoxin inhibition of excitatory synaptic transmission evoked by dorsal root stimulation in rat superficial dorsal horn. *Neuropharmacology* **55:** 860-864.

Motin L, Yasuda T, Schroeder CI, Lewis RJ and Adams DJ (2007) ω-conotoxin CVIB differentially inhibits native and recombinant N- and P/Q-type calcium channels. *Eur J Neurosci* **25:** 435-444.

Mould J, Yasuda T, Schroeder CI, Beedle AM, Doering CJ, Zamponi GW, Adams DJ and Lewis RJ (2004) The $\alpha_2\delta$ auxiliary subunit reduces affinity of ω-conotoxins for recombinant N-type ($Ca_v2.2$) calcium channels. *J Biol Chem* **279:** 34705-34714.

Nadasdi L, Yamashiro D, Chung D, Tarczy-Hornoch K, Adriaenssens P and Ramachandran J (1995) Structure-activity analysis of a *Conus* peptide blocker of N-type neuronal calcium channels. *Biochemistry* **34:** 8076-8081.

Newton RA, Bingham S, Case PC, Sanger GJ and Lawson SN (2001) Dorsal root ganglion neurons show increased expression of the calcium channel $\alpha_2\delta$-1 subunit following partial sciatic nerve injury. *Brain Res Mol Brain Res* **95:** 1-8.

Nielsen KJ, Schroeder T and Lewis R (2000) Structure-activity relationships of ω-conotoxins at N-type voltage-sensitive calcium channels. *J Mol Recognit* **13:** 55-70.

Nowycky MC, Fox AP and Tsien RW (1985) Three types of neuronal calcium channel with different calcium agonist sensitivity. *Nature* **316:** 440-443.

Olivera BM, Miljanich GP, Ramachandran J and Adams ME (1994) Calcium channel diversity and neurotransmitter release: the ω-conotoxins and ω-agatoxins. *Annu Rev Biochem* **63:** 823-867.

Schnolzer M, Alewood P, Jones A, Alewood D and Kent SB (1992) In situ neutralization in Boc-chemistry solid phase peptide synthesis. Rapid, high yield assembly of difficult sequences. *Int J Pept Protein Res* **40:** 180-193.

Schroeder CI, Doering CJ, Zamponi GW and Lewis RJ (2006) N-type calcium channel blockers: novel therapeutics for the treatment of pain. *Med Chem* **2:** 535-543.

MOL #58834

Scott DA, Wright CE and Angus JA (2002) Actions of intrathecal ω-conotoxins CVID, GVIA, MVIIA, and morphine in acute and neuropathic pain in the rat. *Eur J Pharmacol* **451:** 279-286.

Scott WRP, Hunenberger PH, Tironi IG, Mark AE, Billeter SR, Fennen J, Torda AE, Huber T, Kruger P and van Gunsteren WF (1999) The GROMOS biomolecular simulation program package. *Journal of Physical Chemistry A* **103:** 3596-3607.

Snutch TP (2005) Targeting chronic and neuropathic pain: the N-type calcium channel comes of age. *NeuroRx* **2:** 662-670.

Stanley EF (2003) Syntaxin I modulation of presynaptic calcium channel inactivation revealed by botulinum toxin C1. *Eur J Neurosci* **17:** 1303-1305.

Stocker JW, Nadasdi L, Aldrich RW and Tsien RW (1997) Preferential interaction of ω-conotoxins with inactivated N-type Ca^{2+} channels. *J Neurosci* **17:** 3002-3013.

Van Petegem F, Clark KA, Chatelain FC and Minor DL, Jr. (2004) Structure of a complex between a voltage-gated calcium channel β-subunit and an α-subunit domain. *Nature* **429:** 671-675.

Wright CE, Robertson AD, Whorlow SL and Angus JA (2000) Cardiovascular and autonomic effects of ω-conotoxins MVIIA and CVID in conscious rabbits and isolated tissue assays. *Br J Pharmacol* **131:** 1325-1336.

Yasuda T and Adams DJ (2007) Voltage-gated calcium channels in nociception, in *Sensing with Ion Channels* (Martinac B ed) pp 267-298, Springer, Heidelberg.

Yasuda T, Lewis RJ and Adams DJ (2004) Overexpressed $Ca_v\beta3$ inhibits N-type ($Ca_v2.2$) calcium channel currents through a hyperpolarizing shift of ultra-slow and closed-state inactivation. *J Gen Physiol* **123:** 401-416.

MOL #58834

ACKNOWLEDGEMNTS

We thank Dr. T. Yasuda for useful comments and discussion.

MOL #58834

FOOTNOTES[1]

LEGENDS FOR FIGURES

Figure 1. ω-Conotoxin CVIE and CVIF affinity for rat brain calcium channels. pIC_{50} values for CVIE (10.72 ± 0.27 M) and CVIF (10.60 ± 0.41 M) at VGCCs are compared with GVIA and CVID affinities measured from displacement of ^{125}I-GVIA binding to rat brain membranes. Data are means $\pm$ SEM from 4–5 separate experiments, each performed in triplicate.

Figure 2. Inhibition of recombinant N-type ($Ca_v2.2$) VGCCs expressed in *Xenopus* oocytes by ω-conotoxins. **A**, Ba^{2+} currents (I_{Ba}) recorded from oocytes injected with $Ca_v2.2$ VGCC α_{1B-b}, $\alpha_2\delta1$, and β_3 cRNAs. Representative superimposed I_{Ba} obtained in the absence (*top, left and middle*) and presence of 100 nM CVIE (*bottom*, *left*; n = 4) and 100 nM CVIF (*bottom*, middle; n = 5). *Right*: normalized current−voltage relationships in the absence (control) and presence of CVIE and CVIF. Currents were evoked by 200 ms depolarizing voltage steps in 10 mV increments at every 10 s, from a HP of –80 mV (*inset*: voltage protocol). **B**, Representative normalized I_{Ba} traces obtained before (C, control) and after (arrowhead) application of 100 nM ω-conotoxin CVIE, CVIF, or CVIB (*top*), from oocytes injected with $\alpha_{1B-b}/\alpha_2\delta1/\beta_3$ or α_{1B-b}/β_3 $Ca_v2.2$ VGCC cRNAs. Currents evoked by 200 ms step depolarizations to 0 mV from a HP of –80 mV (*inset*: voltage protocol). *Bottom*: Cumulative concentration−response curves for the normalized peak I_{Ba} in the presence or absence of the auxiliary $\alpha_2\delta1$ Ca^{2+} channel subunit. In each case, the solid curve is the best fit with the Hill equation (*see* text for IC_{50} values).

Figure 3. Recombinant N-type (Cav2.2) VGCC recovery from block by CVIE and CVIF is voltage dependent. **A**, HP affects peak I_{Ba} amplitude and recovery from block by ω-conotoxin

CVIF. I_{Ba} was evoked by 200-ms, 0.1-Hz depolarizations to 0 mV from HPs of –80 or –125 mV (voltage *insets*) and peak current amplitudes were plotted as a function of time. Representative current traces (*top insets*) are shown at the times indicated by *lower case letters*. Note the slow and incomplete recovery of peak I_{Ba} after CVIF block at –80 mV (*asterisk*). **B**, Voltage dependence of block (*left*) and reversibility of block (*right*) following bath application of 100 nM ω-conotoxin CVIE, CVIF or CVIB. Oocytes were voltage-clamped at the indicated holding potentials, and membrane currents were elicited by 200 ms step depolarizations to 0 mV, applied every 10 s. *Asterisks* denote statistical differences between –125 mV and various HPs (*$p <$ 0.05, one-way ANOVA); the numbers between parentheses indicate the number of experiments.

Figure 4. In *Xenopus* oocytes, the recovery of non-inactivating N-type ($\alpha_{1B-b}/\alpha_2\delta1/\beta_{2a}$) VGCCs from CVIE or CVIF block is reversible. **A**, Representative superimposed traces of I_{Ba} in the absence (c, control; w, wash) and presence of 100 nM CVIE, CVIF, or CVIB (b, block), evoked by 200-ms depolarizing pulses to 0 mV from a HP of –80 mV, at 0.1 Hz. Bars, 1 μA and 100 ms (top); dashed lines indicate zero-current level. The horizontal bars indicate the duration of drug application. Peak current amplitudes were plotted as a function of time (*bottom*). **B**, Similar experiments to those shown in A, with β_3 auxiliary subunits instead of β_{2a}. **C**, Reversibility of block following bath application of 100 nM ω-conotoxin CVIE, CVIF, CVIB, or GVIA seen with $\alpha_{1B-b}/\alpha_2\delta1/\beta_{2a}$, or $\alpha_{1B-b}/\alpha_2\delta1/\beta_3$ VGCCs. The numbers between parentheses indicate the number of experiments. *Asterisks* denote statistical differences (*$p < 0.001$, unpaired Student's t-test). Data marked by "Ref" is from Mould et al. (2004) and represents recovery from block by 1 nM GVIA.

Figure 5. VGCC inhibition by ω-conotoxins CVIE and CVIF and voltage-dependent recovery from block in acutely dissociated rat DRG neurons. **A**, Representative superimposed traces of I_{Ba} obtained in the absence (c, control; w, wash) and presence of 100 nM CVIE or CVIF; *dashed lines* indicate zero-current level. Bars, 1 nA and 100 ms; *insets*: voltage protocols; membrane currents were elicited by 200 ms step depolarizations, applied every 10 s. **B**, Normalized fractions of blocked (*left*) and recovered (*right*) I_{Ba} *versus* the HP. The numbers in parentheses represent the number of cells. *Asterisks* denote statistical differences (*$p < 0.05$, unpaired Student's t-test). **C,** Representative time course of onset and recovery from block of I_{Ba} following application and, respectively, washout of CVIF, at HPs of –80 and –110 mV. The horizontal bar indicates the duration of drug application. Voltage protocol same as in A. **D**, Representative time course of inhibition of peak I_{Ba} by 10 μM nifedipine in the presence of 500 nM CVIB and 1 μM CVIF (n = 2). Horizontal bars indicate the sequence and duration of drug application. Membrane currents were elicited by 200-ms step depolarizations to –10 mV, applied every 15 s, from a HP of –80 mV. Similar results were obtained with CVIE (n = 4). **E,** CVIF does not inhibit low-voltage activated T-type VGCC currents (n = 3). *Dashed lines* indicate zero-current level. *Left*: Representative superimposed T-type Ba^{2+} currents in a DRG neuron (21 pF) elicited by 150 ms step depolarizations in 10 mV increments, applied every 5 s, from a HP of –80 mV ((*inset* voltage protocol). *Right*: Time course of T-type current peak amplitude in a DRG neuron (41 pF) recorded in the absence and presence of 1 μM CVIF. Representative traces at the times indicated by *lower case letters*. Currents elicited by 150-ms step depolarizations, applied every 15 s. (*inset*: voltage protocol). Similar results were obtained with CVIE (*not shown*).

Figure 6. Effect of ω-conotoxins CVIE and CVIF on evoked excitatory postsynaptic currents (EPSCs) in superficial dorsal horn neurons receiving polysynaptic input. **A**, Time course of the inhibition of EPSC amplitude by 100 nM CVIE (*top*) and 100 nM CVIF (*bottom*). EPSCs were elicited by electrically stimulating the dorsal root with 0.1 ms pulses applied every 10 s via a bipolar electrode at room temperature (23-25°C) and peak EPSC amplitude was plotted as a function of time. Data were filtered at 10 kHz, and digitized at 50 kHz. *Insets*: Representative superimposed average of 5 EPSCs recorded at the times indicated by arrowheads. **B**, Normalized fractions of blocked (*left*) and recovered (*right*) EPSCs following application and respective washout of 100 nM CVIE or CVIF. The HP was -80 mV; the numbers in parentheses represent the number of cells.

Figure 7. Intrathecal injection of 1 nM ω-conotoxin CVID, CVIE or CVIF but not saline vehicle (10 µl) completely relieves mechanical allodynia in a nerve injury model of neuropathic pain for up to 4 hours after injection. Broken line indicates pre-surgery baseline paw withdrawal threshold in the paw ipsilateral to the nerve injury. *, + and #, respectively, denote significant difference (in all cases, $p < 0.001$, two-way ANOVA, Bonferroni posthoc test) between treatment and vehicle; the numbers between parentheses indicate the number of experiments).

Figure 8. Distribution of electrostatics surface properties of the ω-conotoxins CVIE (A), CVIF (B), MVIIA (C), MVIIC (D). The electrostatic potential is colored from red (negative charge) to blue (positive charge). All surface representations are prepared in the same orientation. Labeled are residues ω-conotoxins pharmacophore surrounding Y13, which is oriented to point out of the page in the left hand panels.

Figure 9. Superposition of the comparative models of CVIE (thin green ribbon) and CVIF (thin orange ribbon) and the NMR structures of MVIIA (thick blue ribbon) and MVIIC (thick magenta ribbon). The structural alignments were performed based only on the pharmacophore region (shown in sticks).
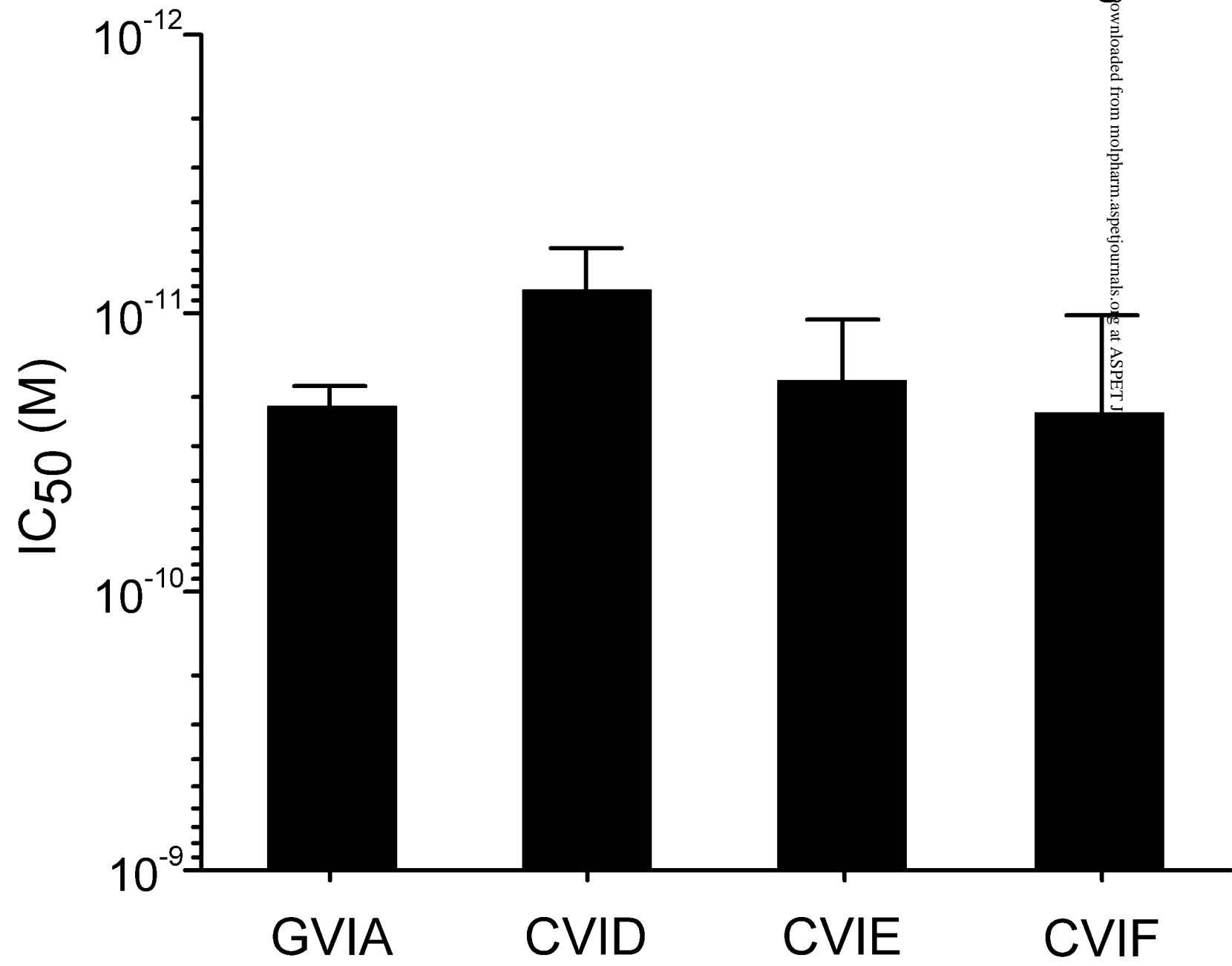
Table I. Amino acid sequence of selected ω-conotoxins from the venom of *Conus catus*.

Conserved cysteine residues are in bold.

Toxin	*Sequence*
MVIIA	**C** K G K G A K **C** S R L M Y D **C** **C** T G S **C** R – – S G K **C** – – NH₂
GVIA	**C** K S O G S S **C** S O T S Y N **C** **C** R – S **C** N O Y T K R **C** Y – NH₂
CVIA	**C** K S T G A S **C** R R T S Y D **C** **C** T G S **C** R – – S G R **C** – – NH₂
CVIB	**C** K G K G A S **C** R K T M Y D **C** **C** R G S **C** R – – S G R **C** – – NH₂
CVID	**C** K S K G A K **C** S K L M Y D **C** **C** S G S **C** S G T V G R **C** – – NH₂
CVIE	**C** K G K G A S **C** R R T S Y D **C** **C** T G S **C** R – – S L R **C** – – NH₂
CVIF	**C** K G K G A S **C** R R T S Y D **C** **C** T G S **C** R – – S G R **C** – – NH₂

Figure 1

Figure 2

Figure 3

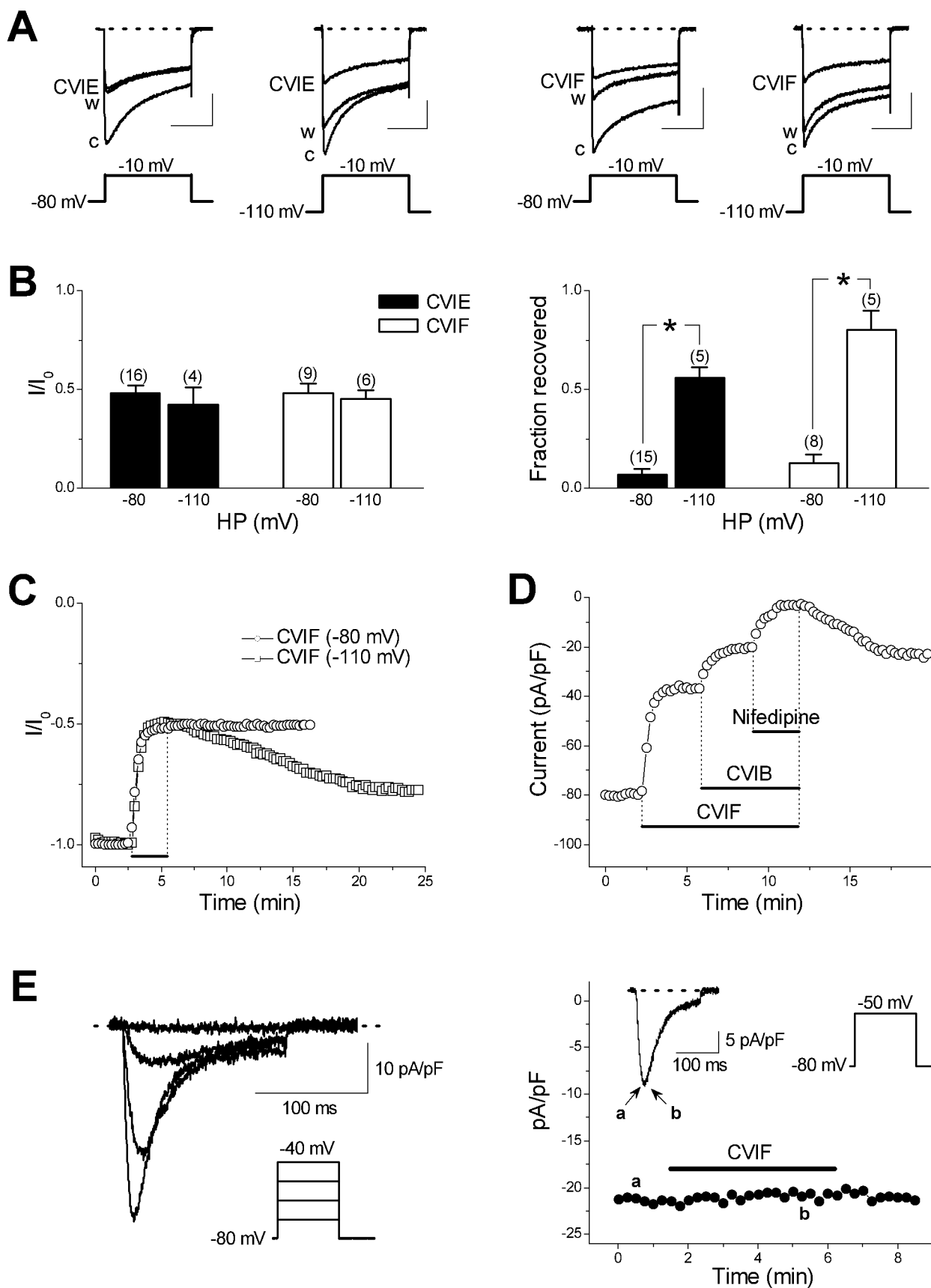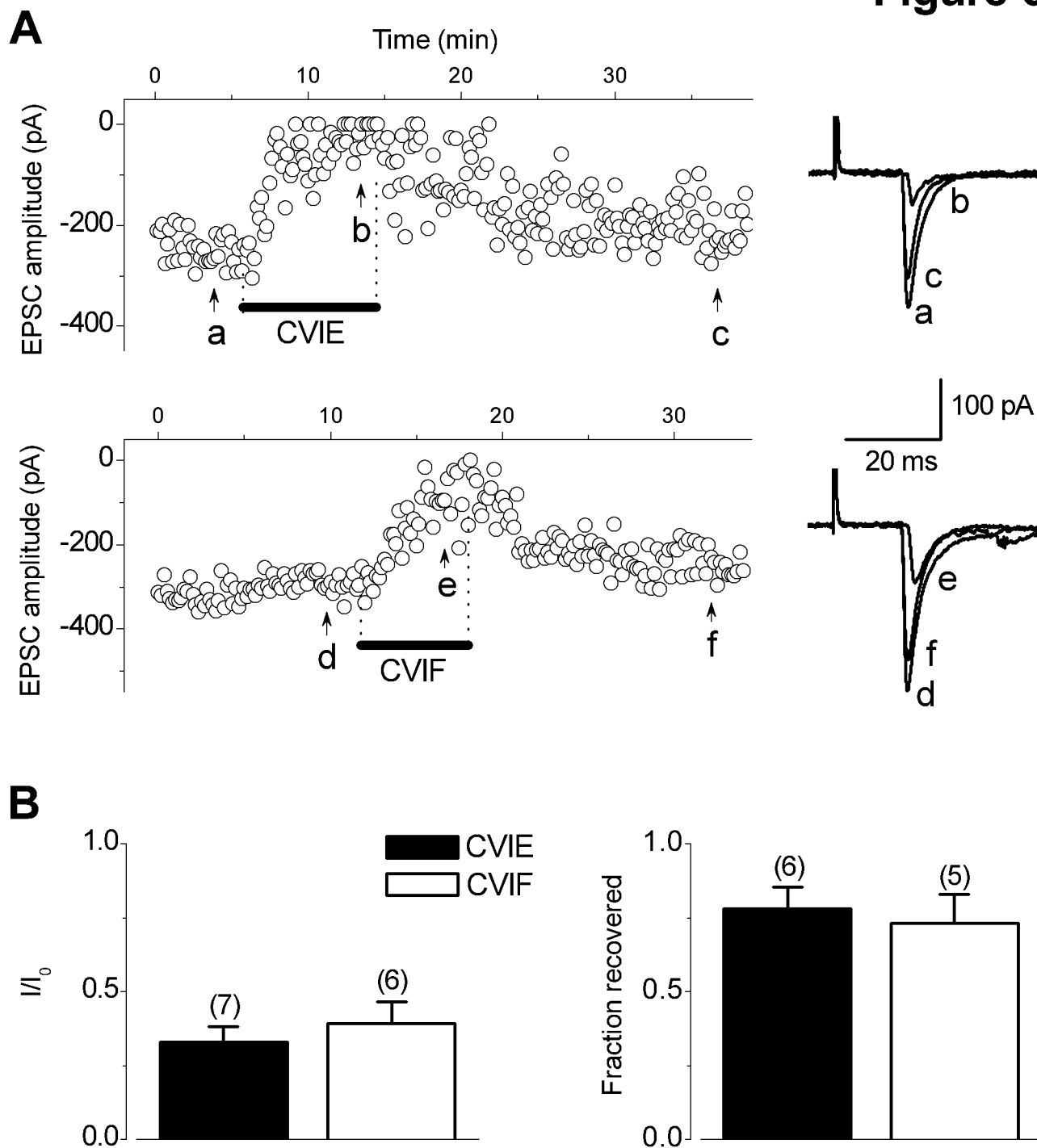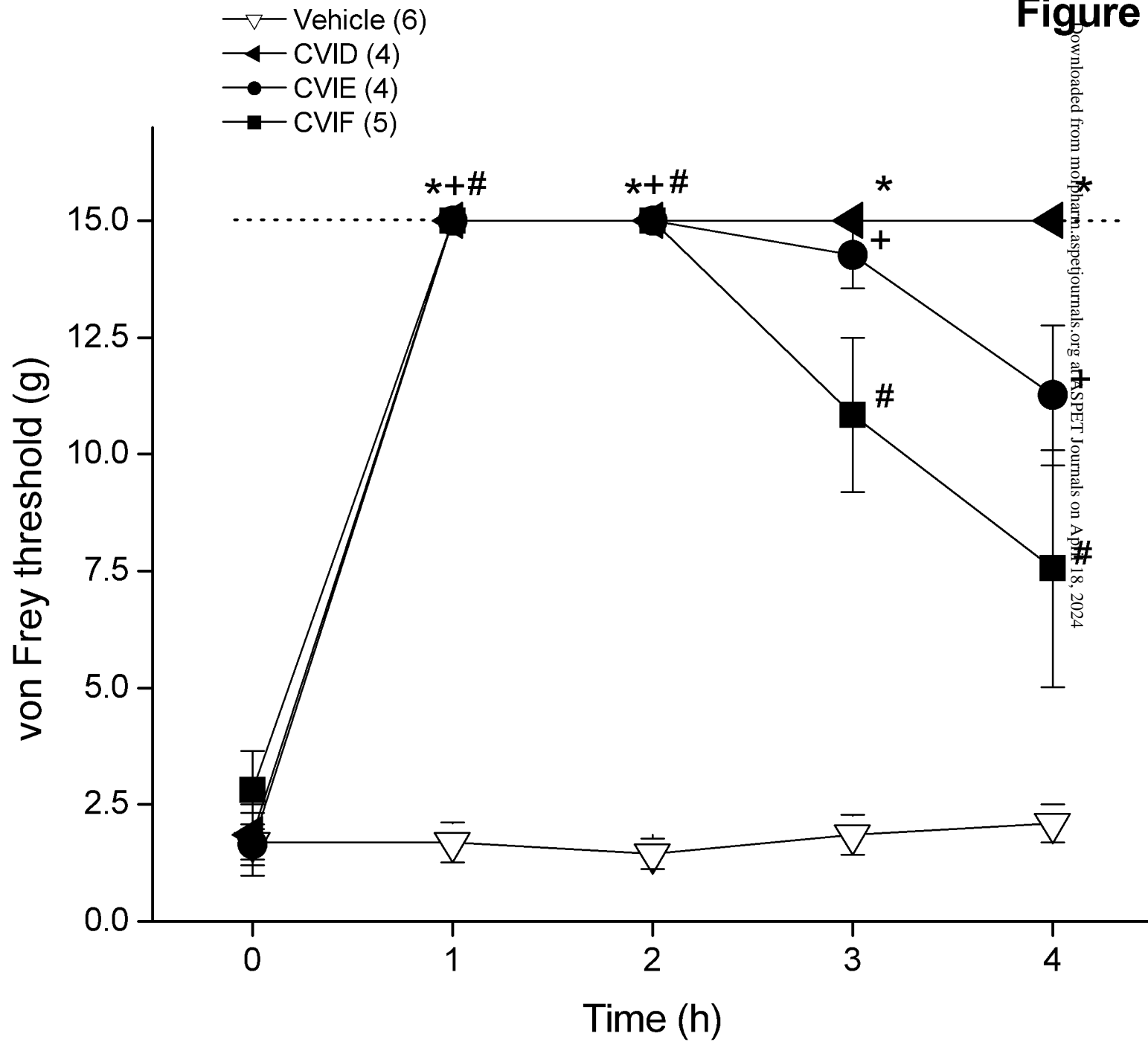**Figure 4**

Figure 5

A

B

C

D

E
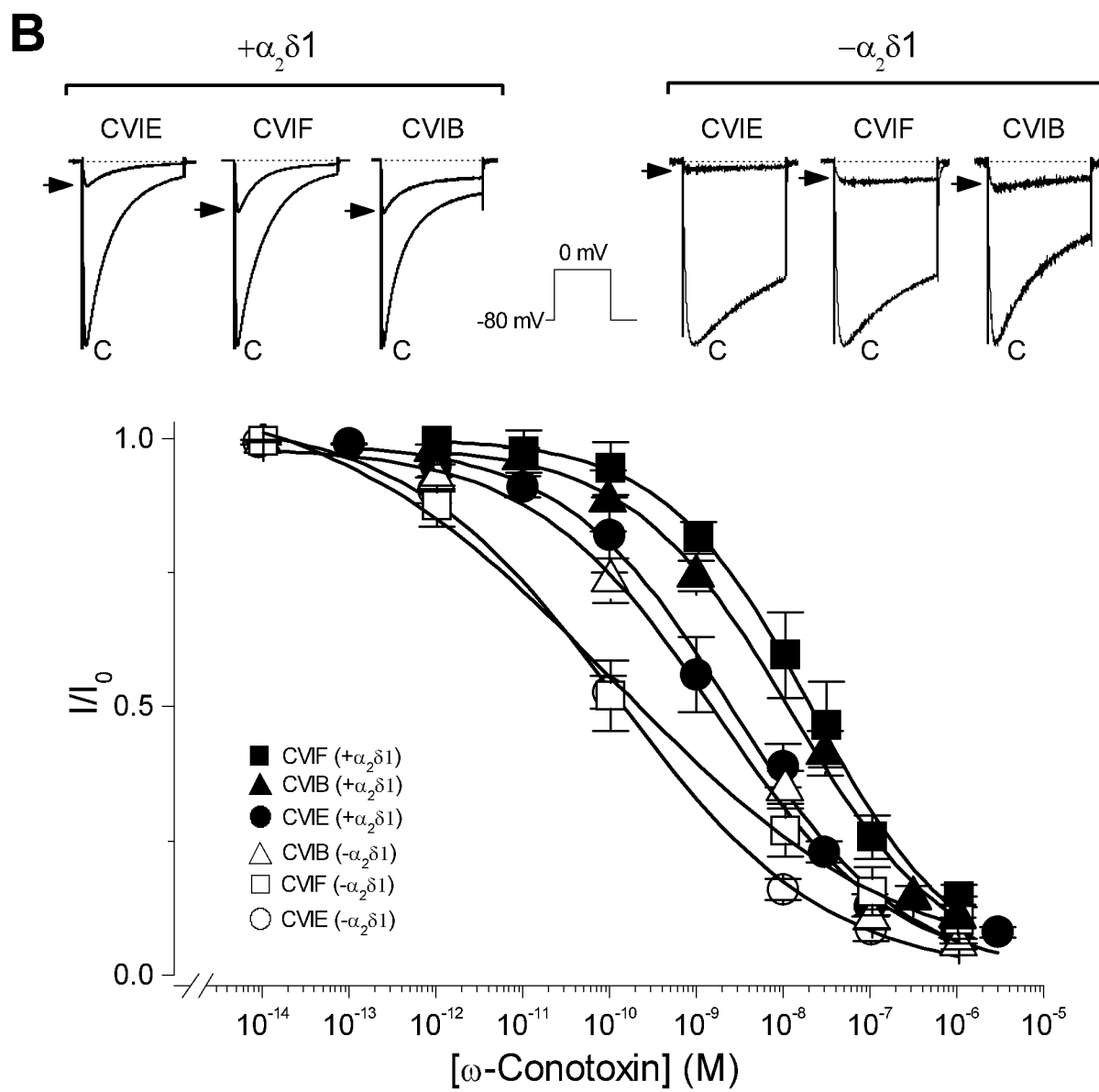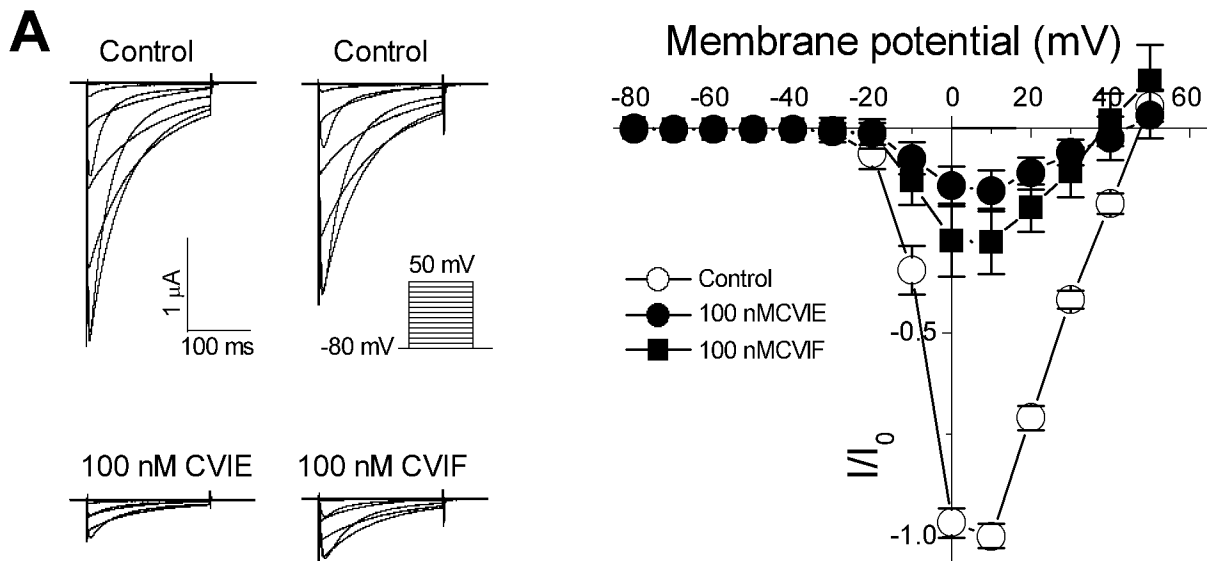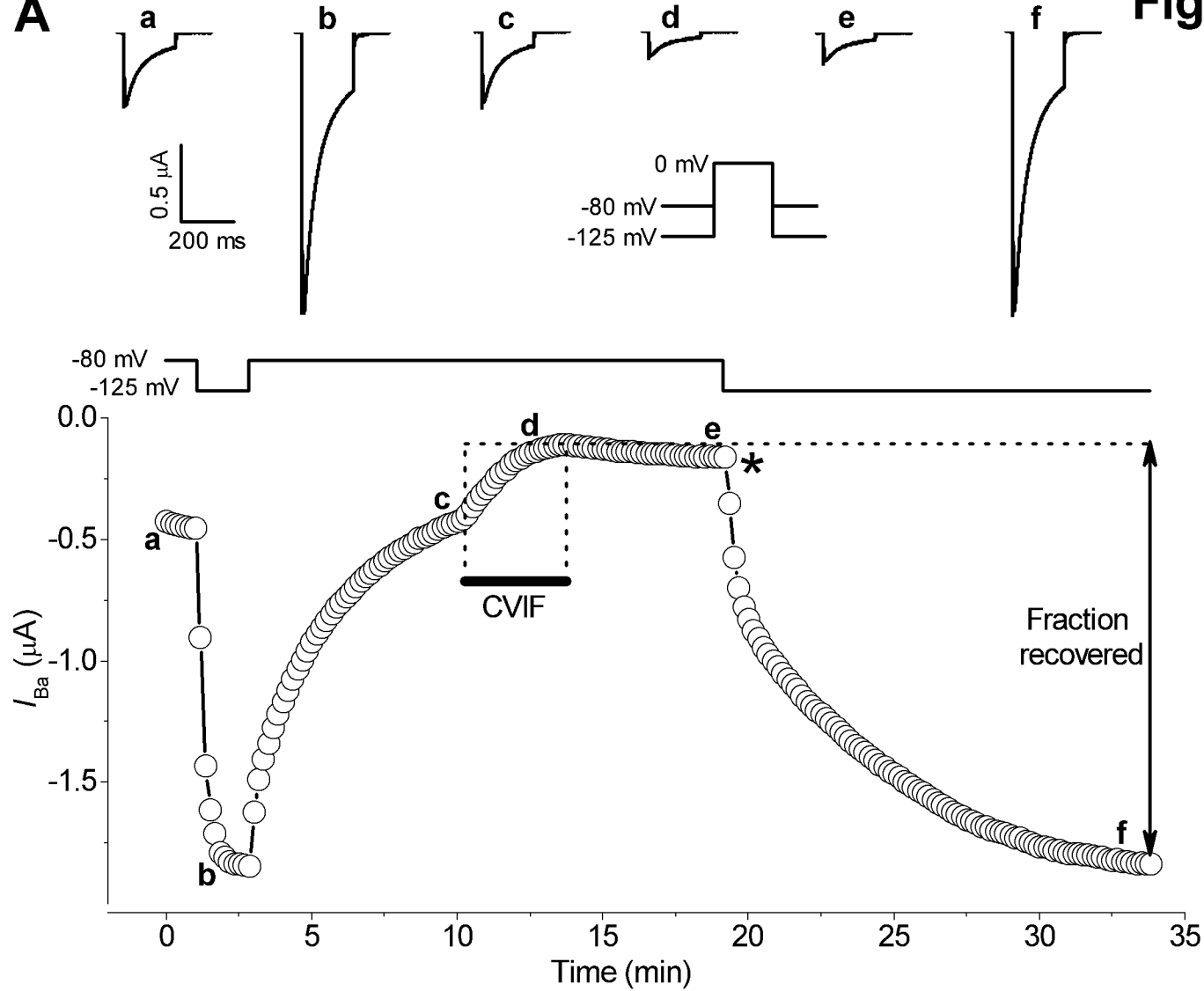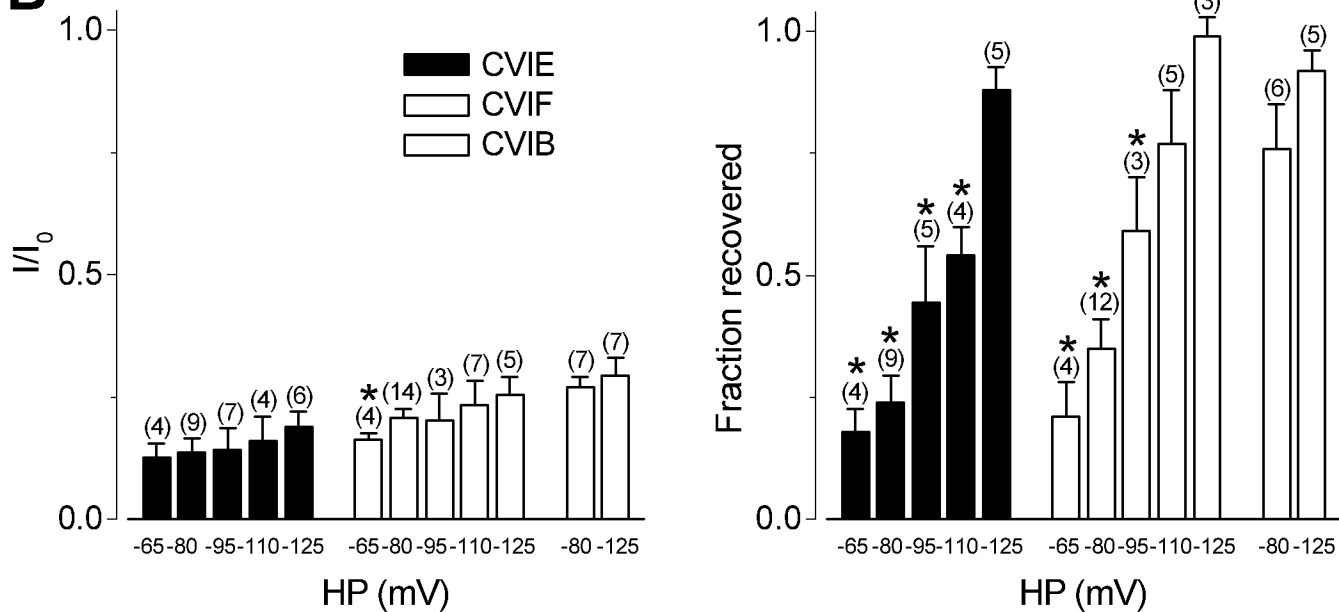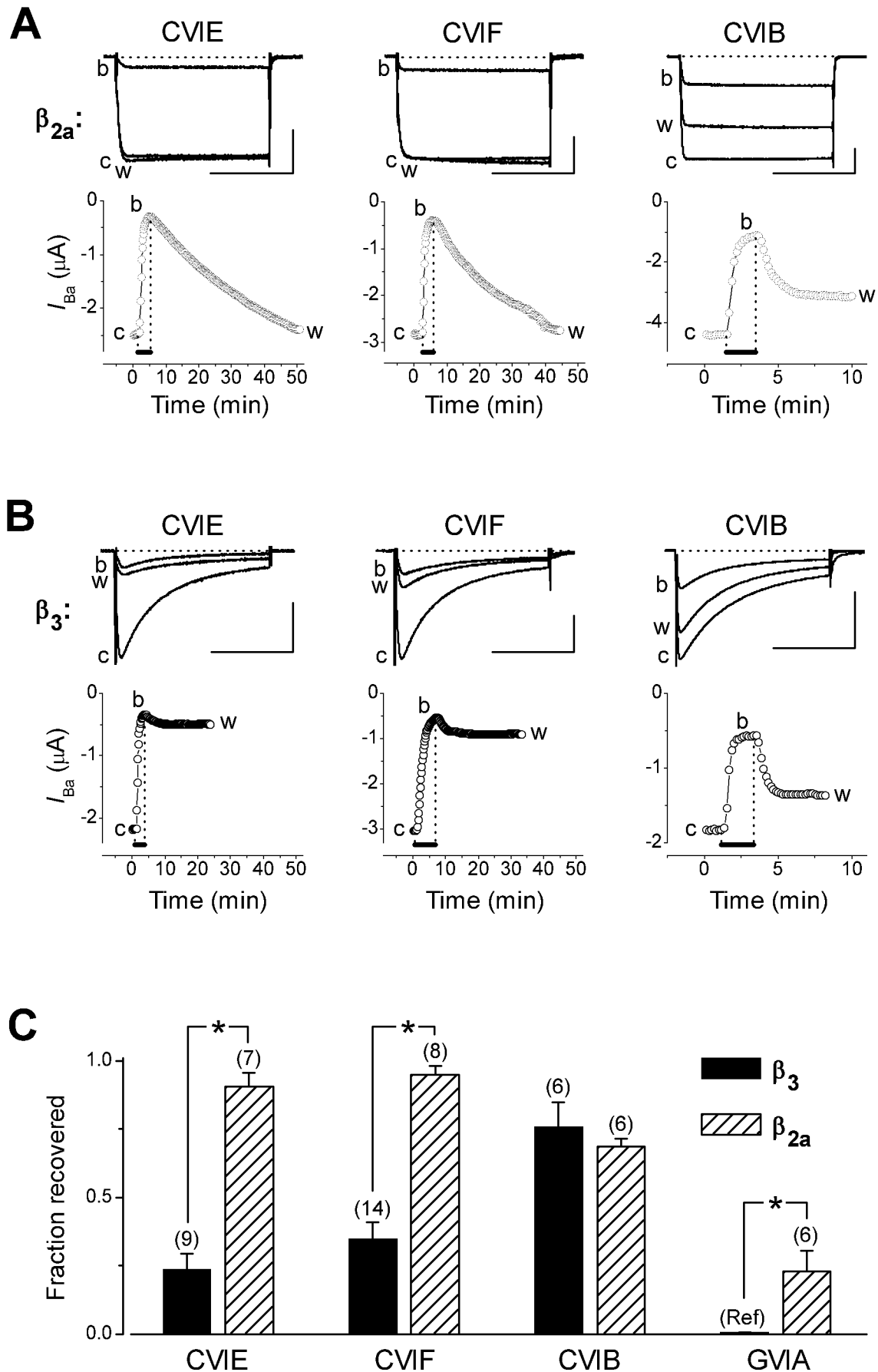
Figure 6

Figure 7

Figure 8

Electrostatics plot

Figure 9